Published in final edited form as:
Thermochim Acta. 2020 ; 686: . doi:10.1016/j.tca.2020.178538.

Heat capacity and decomposition of rimantadine hydrochloride

Ala Bazyleva[a,*], **Eugene Paulechka**[a], **Dzmitry H. Zaitsau**[b], **Andrey V. Blokhin**[c], **Gennady J. Kabo**[c]

[a]Applied Chemicals and Materials Division, National Institute of Standards and Technology, Boulder, CO 80305-3337, USA

[b]Competence Center CALOR, Department Life Light and Matter, University of Rostock, Albert-Einstein-Str. 25, 18059 Rostock, Germany

[c]Chemistry Faculty, Belarusian State University, Leningradskaya 14, Minsk 220030, Belarus

Abstract

Heat capacities of the antiviral drug rimantadine hydrochloride in the crystalline state were measured by adiabatic calorimetry and differential scanning calorimetry in the temperature range from (7 to 453) K. A broad low-enthalpy solid-state phase anomaly was detected between (170 and 250) K. Thermodynamic functions for crystalline rimantadine hydrochloride were derived. Decomposition of the studied compound was probed by the Knudsen effusion method and thermogravimetry with the support of quantum chemical calculations. The enthalpy of decomposition of rimantadine hydrochloride into the corresponding amine and hydrogen chloride was estimated from those data. The thermodynamic functions of the corresponding amine in the ideal gaseous state, including enthalpy of formation, were obtained using statistical thermodynamics with the necessary molecular parameters computed using quantum chemical methods. The enthalpy of formation of crystalline rimantadine hydrochloride was estimated.

Keywords

Rimantadine chloride; heat capacity; thermodynamic properties; decomposition; quantum-chemistry calculations

1. Introduction

An important branch of the chemical industry is specialty chemicals manufacturing (synthetic dyes, drugs, chemical additives, insecticides, etc.). A noticeable interest in this field is directed to adamantane derivatives, whose chemistry has been intensively studied since the middle of the 20th century [1-2]. Compounds from this class have already found numerous applications due to the diversity of their properties: *e.g.*, as

*Corresponding author: A. Bazyleva – Tel.: +1-303-497-5981; ala.bazyleva@nist.gov.

Supporting Information. Experimental heat capacities of crystalline rimantadine hydrochloride measured in an adiabatic calorimeter (Table S1) and a differential scanning calorimeter (Table S2) as well as calculated unscaled vibrational frequencies for rimantadine, rimantadine hydrochloride, and hydrogen chloride (Table S3). This material is available free of charge via the Internet at doi: https://doi.org/10.1016/j.tca.2020.178538

medicines, lubricants, and additives. To date, hundreds of adamantane derivatives have already been studied for pharmacological activity. Some of them are being used as drugs, such as rimantadine, amantadine, memantine, and gludantane [3-6]. However, insufficient thermodynamic property knowledge for these compounds inhibits development of effective, environmentally friendly technologies for their production and limits the possibility of effective property prediction for this class.

This paper is a continuation of a series of publications on condensed-phase thermodynamic properties of adamantane derivatives [7-14]. Rimantadine hydrochloride ($C_{12}H_{22}NCl$, 1-(1-adamantyl)ethanamine hydrochloride, CAS registry number 1501-84-4, Figure 1a), which is produced as a racemic mixture, was selected in this study due to its current use as an antiviral drug [3] and its potential use as an antiparkinsonian medication [15-16]. Rimantadine hydrochloride is structurally similar to another compound (amantadine hydrochloride – Figure 1b) recently studied by us [7]. This similarity allows tracing patterns in changing thermodynamic properties with structural modifications. Besides the crystallographic density of 1.13 g·cm^{-3} obtained by single-crystal X-ray diffraction analysis at 291 K (tetragonal space group $P4_2bc$ with the lattice cell parameters of a = 1.83774 nm, c = 0.75049 nm, and Z = 8) [17], no relevant property data were found for this compound in the literature.

2. Materials and Methods

2.1. Sample preparation

Two samples of rimantadine hydrochloride (racemic mixture) were used in this work (Table 1). One sample used for heat-capacity experiments in an adiabatic calorimeter and in a Knudsen-effusion apparatus was supplied by RUE “Belmedpreparaty” (Minsk, Belarus). The initial mass-fraction purity was not less than 0.99 according to a certified analysis carried out by the manufacturer. The sample was additionally exposed to vacuum at T = 293 K and p = 0.4 kPa for 2 h in order to remove volatile impurities and moisture, if present. The sample was stored in a desiccator over P_2O_5 after the vacuum treatment for at least one week. No further purity analysis was done. Another sample used for heat-capacity experiments in a commercial differential scanning calorimeter (DSC) and for thermogravimetric analysis (TGA) was from Acros Organics (ThermoFisher Scientific, Lot 75749) with the certified mass-fraction purity of 0.95. It was exposed to vacuum at T = 333 K and p = 5 Pa for 2 h to remove any volatile impurities and water. The preliminary sublimation experiments carried out in a TGA apparatus showed total sublimation of the sample without any solid residue. This confirms the absence of any non-volatile inorganic impurities.

The atomic masses of elements recommended by IUPAC (as reported in Table 3 in [18]) were used to derive the molar mass (215.765 g·mol^{-1}).

2.2. Heat-capacity measurements

2.2.1. Adiabatic calorimeter—Heat capacities at saturation pressure ($C_{s,m}$) of crystalline rimantadine hydrochloride were measured in an automatic vacuum adiabatic

calorimeter TAU-10 (Termis, Moscow, Russia) in the temperature range from (7 to 367) K. The calorimeter was described elsewhere [19]. The expanded uncertainty (k = 2) of the $C_{s,m}$ measurements is $0.004 \cdot C_{s,m}$ between T = (20 and 370) K, then, below 20 K, increasing to not more than $0.02 \cdot C_{s,m}$ at 5 K as determined in experiments with benzoic acid, sapphire, and copper in Ref. [19]. The reproducibility for the heat-capacity measurements is better than $0.001 \cdot C_{s,m}$. An iron-rhodium resistance thermometer with R_0 = 50 Ω calibrated for ITS-90 by VNIIFTRI (Mendeleyevo, Moscow Region, Russia) was used for temperature measurements with the standard uncertainty of 0.01 K.

A solid sample of the studied compound (0.6454 g, corrected for buoyancy) was loaded into a titanium calorimetric container ($V \approx 1.1$ cm^3), which was further degassed in vacuum for 0.5 h (residual pressure of ~1 Pa). Helium at $p \approx 15$ kPa and T = 290 K was introduced into the inner free space of the container for facilitation of heat transfer during the measurements. The presence of helium sealed in the container was accounted for in the treatment of the experimental data. The container was sealed using an indium gasket and a titanium lid fixed with a bronze nut. The ratio of the sample heat capacity to the total (sample + container) one was not less than 0.6 in the range of (5 to 20) K, between (0.4 and 0.6) at (20 to 40) K and (0.3 to 0.4) in the remaining region. The experimental parameters were similar to those for amantadine hydrochloride [7]. Heating periods in the experiments varied from (60 to 150) s below 40 K, from (200 to 250) s between T = (40 and 80) K and were fixed at 400 s above 80 K. Periods of thermal relaxation varied from (25 to 100) s for T < 80 K and remained constant at about 150 s in the nitrogen region. Periods of temperature-drift measurements were within (200 to 250) s in the helium region and 300 s for T > 80 K. Temperature steps of the heat-capacity measurements were 1/20 of the absolute temperature for T < 40 K and (1.8 to 2.2) K above 40 K.

A correction for adjustment of $C_{s,m}$ to isobaric heat capacity, $C_{p,m}$, was found to be negligible even at 370 K and, therefore, not taken into consideration.

2.2.2. Differential scanning calorimeter—Isobaric heat capacity of crystalline rimantadine hydrochloride from (243 to 453) K was determined with the use of a heat-compensation technique in a Perkin Elmer Pyrus DSC 1. Dry nitrogen (dew point temperature below 160 K) with the flow rate of 0.8 L·h^{-1} was used as a purge gas. The temperature calibration of the calorimeter was conducted with indium, tin and lead of high purity (>0.999 mass-fraction purity). Temperature was measured with the standard uncertainty of 0.2 K. Calorimetric aluminum pans (catalog number 0219-0041) and samples were weighed with a Sartorius MSE3.6P-000-DM microbalance with the standard uncertainty of $5 \cdot 10^{-6}$ g. Two samples of 16.349 mg and 16.462 mg (corrected for buoyancy) were used. No mass loss from the calorimetric pans was detected after the DSC experiments.

As recommended by the manufacturer, the studied temperature range was divided into several 50 K scanning series for heat capacity measurements with the heating rate of 10 K·min^{-1}. The following three-step procedure was applied: the first series of thermal scans was done for an empty pan; in the second step, thermal scans were done for a reference sample (sapphire); during the third step, thermal scans were carried out for a vacuum-sealed sample of the studied compound. The same pan was used in each step. Eight

runs were conducted for each sample, and the final heat capacities were averaged within 1 K intervals. The heat capacity was derived with the Perkin Elmer software. The heat capacity determination technique was tested with a reference sample of benzoic acid by Parr Instrument Company. In the temperature range 314 K to 350 K, the experimental values agreed with the reference values [20] within ±1 %. The expanded uncertainty ($k = 2$) for the heat capacity measured by this method was thus estimated to be $0.02 \cdot C_{s,m}$.

2.3. Decomposition analysis

2.3.1. Knudsen's effusion method—Effusion measurements for crystalline rimantadine hydrochloride in the temperature range (393 to 458) K were carried out in an experimental set-up with a high-temperature copper block thermostat described previously [21]. Temperature was measured with a platinum resistance thermometer ($R_0 = 10\ \Omega$). The standard uncertainty for temperature determination was estimated to be 0.05 K. Residual pressure in the system was maintained below 10^{-3} Pa with a diffusion vacuum pump.

Crystalline samples of the studied compound were loaded into a cylindrical stainless-steel cell with 10.0 mm height and 10.0 mm internal diameter. Samples of approximately 0.5 g mass were used for the experiments, with periodical replenishing after three to five experiments. In order to facilitate heat transfer, the sample was pressed against the whole inner surface of the cell with a stainless-steel rod. Three nickel membranes with different foil thickness (l) and orifice diameters (d_{or}) were used. The mass losses of the studied compound from the cell through the orifice after each exposure to high vacuum were measured with the use of a Mettler Toledo AG 245 electronic balance with a repeatability of $2 \cdot 10^{-5}$ g (device specification).

2.3.2. Thermogravimetric analysis (TGA)—The sublimation / thermal degradation of rimantadine hydrochloride was studied in Perkin Elmer TGA 6. Dry nitrogen (dew point temperature below 160 K) with the flow rate of 200 $mL \cdot min^{-1}$ was used as a purge gas. A small amount of sample (2 mg to 3 mg) was placed in a 40 μL aluminim DSC pan from Mettler Toledo. The pan lid was pierced with a needle of 0.4 mm diameter, and the pan with the sample was sealed with a crucible sealing press. The mass-loss rate was determined in scanning mode with a heating rate of 5 $K \cdot min^{-1}$. The temperature calibration of the device was carried out utilizing the Curie points of Alumel, nickel, and Perkalloy reference samples. The reference samples of Alumel and Perkalloy were from Perkin Elmer, and the reference sample of nickel (0.99995 mass-fraction purity) was from MaTecK. The standard uncertainty for temperature determination was 2 K. The mass determination was calibrated with a reference weight of 100 mg. The standard uncertainty in the mass determination was estimated to be $5 \cdot 10^{-6}$ g.

2.3.3. FTIR-ATR analysis—Fourier-transform infrared spectroscopy (FTIR) analysis of the samples studied with the TGA technique was carried out with a Nicolet 380 FT-IR spectrometer in a diamond Attenuated Total Reflection (ATR) module. The optical resolution of the device is 1 cm^{-1} and wavenumber precision is 0.01 cm^{-1}.

3. Computations

The rimantadine molecule has two symmetric tops, methyl and adamantyl, and an asymmetric NH_2 top. Optimization of geometries and calculation of vibrational frequencies and rotational potentials were performed using B3LYP hybrid density functional with the def2-TZVP basis set and D3(BJ) correction [22-25]. Parameters of the symmetric tops were found for the most stable conformer formed by rotation of the NH_2 top. The rotational barriers and energies of the NH_2 conformers were evaluated with the 2016 version of local CCSD(T) by Kallay et al. [26-28] and aug-cc-pVQZ basis set [29, 30] using the B3LYP-D3(BJ)/def2-TZVP geometries. In the calculations for the ionic pair and HCl, the basis set aug-cc-pV(Q+d)Z [31, 32] was used for Cl. DFT calculations were performed with the Gaussian 16 package [33]. Local CCSD(T) calculations were carried out with MRCC (May 23, 2018 release) [28].

Contributions of overall rotation to thermodynamic functions were treated with the classical rigid-rotor approximation [34]. Reduced moments of inertia of the tops were calculated in a multiple-top approximation, as described by Pitzer [35]. Vibrational frequencies obtained from quantum-chemical calculations are typically higher than the experimental ones. To achieve quantitative predictions, the frequencies were scaled by 0.990 for zero-point vibrational energies (ZPVE) [36]. In the calculation of thermodynamic functions, the scaling factors of 0.96 for hydrogen stretches and 0.985 for all other modes (*i.e.*, below 2800 cm^{-1}) were applied.

The enthalpy of formation of the amine at T = 298.15 K was found with the equation:

$$\Delta_f H^\circ = E + \mathrm{ZPVE} + \Delta_0^T H - \sum\nolimits_{\mathrm{types}} n_i h_i \quad (1)$$

where E is the total energy of the amine molecule, $\Delta_0^T H$ is the thermal increment from 0 K to T; n_i are the numbers of atoms (C, H, and N) in the molecule; h_i are the effective enthalpies of the atoms. The E value was calculated at the local CCSD(T)/aug-cc-pVQZ// B3LYP-D3(BJ)/def2-TZVP theory level. $\Delta_0^T H$ was found as described below. The effective enthalpies of the atoms, h(C) = −99910.32 kJ·mol^{-1}, h(H) = −1524.23 kJ·mol^{-1}, and h(N) = −143612.32 kJ·mol^{-1}, were taken from [36]. These parameters were originally derived for the molecular geometries calculated at the DF-MP2/aug-cc-pVQZ theory level. However, based on the results [37], we believe this inconsistency will introduce an error of a few tenths kJ·mol^{-1} for the amine which is negligible compared to the expected combined uncertainty.

4. Results

4.1. Thermodynamic properties of crystalline rimantadine hydrochloride

Experimental molar heat capacities of crystalline rimantadine hydrochloride measured in the adiabatic calorimeter and the differential scanning calorimeter described in Section 2.2 are shown in Figure 2 and are summarized in Tables S1 and S2 of the Supporting

Information, respectively. For comparison, Figure 2 also includes the heat capacity of amantadine hydrochloride measured previously [7].

The data for rimantadine hydrochloride from both calorimeters are in excellent agreement: within 0.6% between 243 K and 260 K and 0.3% from 260 K to 367 K, which supports reliability of the reported results. The largest difference between the DSC and adiabatic calorimetry results occurs in the range 243 K to 255 K, where the end of a phase anomaly is detected by adiabatic calorimetry.

As expected from the molecular structures, the heat capacity of rimantadine hydrochloride is larger than that of amantadine hydrochloride at all temperatures outside of phase transitions (Figure 2, including the enlarged low-temperature region in the inset). For example, the difference in heat capacities of rimantadine hydrochloride and amantadine hydrochloride at 298.15 K is 51.3 J K^{-1}·mol^{-1}, which is consistent with a typical contribution from two additional carbon segments in alkyl chains for other organic compounds.

A solid-phase hump-shaped anomaly was observed between (170 and 250) K for rimantadine hydrochloride. This phase anomaly is reproducible, as can be seen from the repeated measurement series given in Table S1. Based on its shape, this anomaly cannot be considered as a first-order solid-phase transition, hence, only excess enthalpy and excess entropy were derived through integration of excess heat capacity (Figure 3): ΔH_m = 0.236 ± 0.024 kJ·mol^{-1} and ΔS_m = 1.10 ± 0.11 J K^{-1}·mol^{-1}. It was found in [17] that exposing crystalline rimantadine hydrochloride to low temperatures (down to around (150 to 180) K) resulted in an increase of mosaicity of the sample. The observed phase anomaly may be responsible for the observed degradation of single crystals. It should also be noted that this anomaly is similar in shape and size to that observed in amantadine hydrochloride (Figure 3), but it appears in rimantadine hydrochloride at higher temperatures and it does not contain any sharp transitions in the middle. Rimantadine hydrochloride and amantadine hydrochloride exhibit similar molecular packing in the crystal, as demonstrated in [17] and [38]: both compounds have parallel rectangular polar channels in the structure. Hence, the phase anomalies in both compounds are likely to be of the same nature.

The heat capacities above 7 K were smoothed with the use of overlapping polynomials whose coefficients were determined by least-squares fitting. In the temperature range where the two methods overlapped, the weighted least-squares method was used. The weights of the experimental points were equal to the reciprocal of the squared relative uncertainties of the methods. Below 7 K, the heat capacities were extrapolated with the following equation including one Debye heat-capacity function with three degrees of freedom, D_3, and one Einstein heat-capacity function with one degree of freedom, E:

$$C_{p,m} = D_3(\langle\Theta_D\rangle / T) + E(\langle\Theta_E\rangle / T), \quad (2)$$

where the average Debye and Einstein characteristic temperatures were derived to be $\langle\Theta_D\rangle$ = 69.3 K and $\langle\Theta_E\rangle$ = 71.8 K, respectively, using the non-linear least-squares fit of the experimental heat capacities between (7.0 to 9.2) K.

The thermodynamic functions for rimantadine hydrochloride in the condensed state from (5 to 453) K were derived from the smoothed heat capacities. Table 2 summarizes the thermodynamic functions.

4.2. Decomposition study

The mass-loss results obtained in the Knudsen effusion apparatus for crystalline rimantadine hydrochloride are summarized in Table 3. The saturation pressure p_{sat} is proportional to

$$p_{sat} \sim \sqrt{T}\,(\Delta m / \tau)\, S_{or}^{-1}, \quad (3)$$

where T is the experimental temperature, Δm is the mass loss over time τ, S_{or} is the orifice area. The logarithm of the right-hand side of Eq. (3) is plotted as a function of reciprocal temperature in Figure 4. The step-like behavior seen in Figure 4 is due to the undersaturation phenomenon in the Knudsen cell (as shown previously [7]), which causes the pressure in the cell to be lower than the corresponding equilibrium pressure. The difference depends on the orifice size and weakly depends on temperature. Hence, the temperature slopes of the pressures are nearly unaffected by this undersaturation.

The apparent enthalpy of sublimation from the slopes of $\ln\left[\sqrt{T}\,(\Delta m / \tau)\, S_{or}^{-1}\right]$ vs $1/T$ for each membrane individually increases with temperature to be 105.1 kJ·mol^{-1} at an average temperature of 408 K, 106.6 kJ·mol^{-1} at 423 K, and 114.3 kJ·mol^{-1} at 446 K. This increase is not consistent with the heat-capacity difference of the decomposition/sublimation reaction expected for this compound:

$$C_{12}H_{22}NCl\,(cr) \rightleftarrows C_{12}H_{21}N\,(gas) + HCl\,(gas) \quad (4)$$

The heat-capacity change in this reaction was estimated from the heat capacities of crystalline rimantadine hydrochloride from Table 2, gaseous rimantadine (see Section 4.3), and gaseous HCl from the CODATA tables [39] to be −19 J·K^{-1}·mol^{-1} at 298.15 K and −24 J·K^{-1}·mol^{-1} at 400 K. With these heat-capacity changes, the enthalpy of reaction (4) should decrease with temperature, which is the opposite to what is seen in Figure 4. Moreover, if one attempts the same approach for treating the effusion results as the one developed in [7] for amantadine hydrochloride with accounting for both gas anisotropy and undersaturation in the Knudsen cell, the situation with the slopes is not improved.

TGA results (Figure 5) also show the increasing enthalpy change associated with the mass loss with increasing temperature. At least two decomposition processes are seen for this compound in the studied temperature range.

We assume that the linear dependence of $\ln(T^{0.5}\mathrm{d}\alpha/\mathrm{d}t)$ vs T^{-1} in the temperature interval 500 to 590 K for the rate of 5 K·min^{-1} (Figure 5) corresponds to the chemical process for equilibrium between gas and solid phase. Above this temperature the deviation from the linear dependence corresponds to another chemical process. No sample residue was observed in the pan after the scanning run in TGA. This implies that the decomposition products are more volatile than the initial sample. FTIR-ATR analysis of the initial sample

and the condensate on the cold (~300 K) lid of the TGA device was carried out (Figure 6). The difference in IR spectra for the initial sample and the condensate is minimal and, correspondingly, the main mass loss corresponds to the equilibrium between solid and gas phases. The products of the second process were not detected on the lid probably due to higher volatility in comparison to rimantadine hydrochloride. One would expect that, at reduced heating rates (equivalent to kelvins per hour in effusion experiments) and a smaller relative orifice size, the high-temperature process would be detectable at lower temperatures, affecting the effusion results. The approach from Ref. [7] cannot be applied for rimantadine hydrochloride, since the equilibrium partial vapor pressures of rimantadine and hydrogen chloride are not available from the effusion results.

The enthalpy change of the mass-loss process estimated from the slope in region I of the TGA curve in Figure 5 (109 $kJ \cdot mol^{-1}$ at 540 K) is consistent with the values derived from the Knudsen effusion in Figure 4. This means that similar processes occur in both experiments. Based on the TGA results, one can conclude that only one process dominates at low temperatures. The chemical analysis results of the decomposition products from the low-temperature end are consistent with reaction (4). Consequently, the enthalpy of the decomposition reaction (4) can be estimated from the temperature dependence of mass losses obtained with the membrane with the largest orifice, *i.e.*, at the low-temperature end, where no effect of another decomposition process is expected. However, the entropy of decomposition and the equilibrium constant of reaction (4) cannot be obtained from the effusion results, since significant undersaturation is expected for the experiments with the largest orifice, as it is seen for the experiments with that membrane for a structurally similar amantadine hydrochloride. The possibility to derive the enthalpy of reaction (4) from the temperature dependence of mass losses can be demonstrated as follows.

Since rimantadine hydrochloride is a racemic compound (it was shown in [17] that a single crystal includes 1:1 ratio of R- and S-isomers), its decomposition reaction should be written as the following stereospecific chemical reaction:

$$\begin{aligned} &0.5(\text{R-}C_{12}H_{22}NCl)^{*}(\text{S-}C_{12}H_{22}NCl)\,(cr) \rightleftarrows \\ &\rightleftarrows 0.5\,\text{R-}C_{12}H_{21}N\,(gas) + 0.5\,\text{S-}C_{12}H_{21}N\,(gas) + HCl\,(gas)\,. \end{aligned} \tag{5}$$

The equilibrium constant for this reaction ($K°$) can be expressed as:

$$K^{o} = \left(p_{eq,\,R-amine} \,/\, p^{o}\right)^{0.5}\left(p_{eq,\,S-amine} \,/\, p^{o}\right)^{0.5}\left(p_{eq,HCl} \,/\, p^{o}\right), \tag{6}$$

where $p°$ is the standard pressure (10^5 Pa); $p_{eq,R\text{-amine}}$, $p_{eq,S\text{-amine}}$ and $p_{eq,HCl}$ are the equilibrium partial pressures of R-rimantadine and S-rimantadine and hydrogen chloride, respectively. Since this is a reacemic compound with 1:1 ratio and the effusion of both isomers will be with the same rate, the equilibrium pressures of both forms are the same:

$$K^{o} = \left(p_{eq,\,R-amine} \,/\, p^{o}\right)\left(p_{eq,HCl} \,/\, p^{o}\right) = \left(p_{eq,total\ amine} \,/\, (2p^{o})\right)\left(p_{eq,HCl} \,/\, p^{o}\right), \tag{7}$$

where $p_{eq,total\ amine} = p_{eq,R\text{-amine}} + p_{eq,S\text{-amine}} = 2p_{eq,R\text{-amine}}$ is the total equilibrium pressure of the amine form.

The enthalpy of reaction (5) can be derived as:

$$\partial \ln (K^{o}) \,/\, \partial (1 \,/\, T) = \partial \ln (p_{\mathrm{eq,total\ amine}} \cdot p_{\mathrm{eq,HCl}}) \,/\, \partial (1 \,/\, T) = -\Delta_{r} H_{m}^{o}(T) \,/\, R \ . \quad (8)$$

Thus, the enthalpy of reaction (5) is equivalent to the enthalpy of reaction (4), so that all further calculations are for non-stereospecific reaction (4).

The equilibrium partial pressures of the amine form and HCl in the effusion cell can be derived as described in [7] to be:

$$p_{\mathrm{eq,total\ amine}} = \frac{\sqrt{2\pi RT\, M_{\mathrm{amine}}}}{k_{\mathrm{amine}} S_{\mathrm{or}} (M_{\mathrm{amine}} + M_{\mathrm{HCl}})} \left(\frac{\Delta m_{\mathrm{tot}}}{\tau} \right) (1 + A\, k_{\mathrm{amine}} S_{\mathrm{or}}) \quad (9)$$

$$p_{\mathrm{eq,HCl}} = \frac{\sqrt{2\pi RT\, M_{\mathrm{HCl}}}}{k_{\mathrm{HCl}} S_{\mathrm{or}} (M_{\mathrm{amine}} + M_{\mathrm{HCl}})} \left(\frac{\Delta m_{\mathrm{tot}}}{\tau} \right) (1 + A\, k_{\mathrm{HCl}} S_{\mathrm{or}}) \quad (10)$$

where S_{or} is the effusion orifice area; k_{amine} and k_{HCl} are the transmission probabilities for the molecules of rimantadine and HCl through the orifice, respectively; T is the average temperature in the effusion experiment; M_{amine} and M_{HCl} are the molar masses of the effusing vapors of rimantadine and HCl; R is the gas constant (R = 8.3144626 $\mathrm{J{\cdot}K^{-1}{\cdot}moly^{-1}}$). To simplify the derivation, it was assumed that the transmission probabilities do not depend on temperature. The assumption is based on the calculations for amantadine hydrochloride in [7], where the change of k with temperature contributes only about 3 $\mathrm{kJ{\cdot}mol^{-1}}$ to the enthalpy of the decomposition reaction for that membrane. Moreover, this simplified approach produces data more consistent with TGA. No reasonable explanation of such behavior has been found by us.

With Equations (9)-(10), we can rearrange Equation (8) as:

$$\partial \ln \left[T \left(\frac{\Delta m_{\mathrm{tot}}}{\tau} \right)^{2} \right] \,/\, \partial (1 \,/\, T) = -\Delta_{r} H_{m}^{o}(T) \,/\, R \ . \quad (11)$$

The average enthalpy of reaction (4) was derived from experiments #1-#7 from Table 3 to be $\Delta_{r} H_{m}^{o}$ (408 K)= (210 ± 7) $\mathrm{kJ{\cdot}mol^{-1}}$, where the expanded uncertainty with 0.95 level of confidence is estimated from the regression of the experimental data and a possible systematic error from the above assumption on the transmission probability. The enthalpy of the decomposition reaction (4) was adjusted from 408 K to 298.15 K with the use of the average heat-capacity change of reaction (4) in this temperature range of (−22 $\mathrm{J{\cdot}K^{-1}{\cdot}mol^{-1}}$): $\Delta_{r} H_{m}^{o}$(408 K)= (213 ± 7) $\mathrm{kJ{\cdot}mol^{-1}}$.

4.3. Computations of thermodynamic properties of rimantadine and rimantadine hydrochloride

Computed rotational constants are listed in Table 4. The symmetry number equals one for all considered species. In the amine, the contributions of torsional modes to the thermodynamic

functions were calculated from energy levels of the corresponding independent rigid rotors obtained according to the procedure described in Appendix B in Ref. [40]. For the methyl and adamantyl tops, the potential function was assumed to have the form

$$V(\varphi) = \frac{V_0}{2}(1 + \cos 3\varphi) \tag{12}$$

where φ is a phase angle. The V_0 parameters where found using single-point local CCSD(T)/aug-cc-pVQZ//B3LYP-D3(BJ)/def2-TZVP calculations to be 5.77 and 13.77 kJ·mol^{-1} for the methyl and adamantyl tops, respectively. The reduced moments of inertia (5.179 and 84.31)·10^{-47} kg·m^2, respectively) were assumed to be constant and equal to those in conformer 2. The extreme points on a potential energy curve for the NH_2 top were obtained in a similar way. These points were fitted with the equation:

$$\begin{aligned} V_{\mathrm{NH2}}(\varphi) \ / \ \mathrm{J \cdot mol^{-1}} = 5712 - 2128\cos\varphi - 1693\cos 2\varphi + 4180\cos 3\varphi + \\ + 138\sin\varphi + 1036\sin 2\varphi - 310\sin 3\varphi \end{aligned} \tag{13}$$

The reduced moment of inertia of this top was found to be 2.955·10^{-47} kg·m^2.

The contributions of remaining vibrations were determined using the canonical harmonic oscillator approximation [34]. The computed vibrational frequencies are reported in Table S3 of the Supporting Information. The resulting thermodynamic functions of the amine, including the enthalpies of formation are presented in Table 5. The thermodynamic functions of the elements necessary for the calculation of the enthalpy of formation and the Gibbs energy of formation at different temperatures were taken from Ref. [39]. At T = 298.15 K, the expanded uncertainty (k = 2) of the gas-phase enthalpy of formation of the amine is $U(\Delta_f H^\circ_m)$ = 2.9 kJ·mol^{-1} [37].

The enthalpy of the rimantadine hydrochloride decomposition reaction in the gas phase,

$$\mathrm{C_{12}H_{22}NCl\,(gas) = C_{12}H_{21}N\,(gas) + HCl\,(gas)} \tag{14}$$

was found using the total energies of the participants computed at the LCCSD(T)/aug-cc-pVQZ//B3LYP-D3(BJ)/def2-TZVP level of theory. Contributions of the torsional frequencies to the thermal part of enthalpy $\Delta_0^T H$ were evaluated as the harmonic ones corrected for existence of several conformers. This simplified approximation can be used because the expected errors in the amine and salt are cancelled. The basis-set superposition error was found using the counterpoise correction procedure [41],

$$\Delta E_{\mathrm{BSSE}} = E(\mathrm{salt}) - (E(\mathrm{amine}) + \Delta E^*(\mathrm{amine})) - (E(\mathrm{HCl}) + \Delta E^*(\mathrm{HCl})), \tag{15}$$

where ΔE* is the single-point energy difference between a species calculated with a basis set of the ionic pair and the species itself. To calculate ΔE*, the species' geometry of conformer 2 of the ionic pair was used. At T = 298.15 K, the gas-phase dissociation enthalpy was found to be $\Delta_{\mathrm{dis}} H^\circ_m$ = 38.8 kJ·mol^{-1}. Per our estimate, the expanded uncertainty (k = 2) of this value is about $U(\Delta_{\mathrm{dis}} H^\circ_m)$ = 1 kJ·mol^{-1}. Combination of this value with the enthalpies of

formation of the gaseous amine (Table 5) and HCl (−92.31 ± 0.10) kJ·mol^{-1} [39] results in the enthalpy of formation for gaseous rimantadine hydrochloride adduct: $\Delta_f H^\circ_m$(salt(g)) = (−299.7 ± 3.1) kJ·mol^{-1}.

The enthalpy of heterogeneous dissociation (reaction (4)) estimated in Section 4.2 allows us to estimate the enthalpy of formation of rimantadine hydrochloride in the crystalline state at 298.15 K. The enthalpies of formation of gaseous rimantadine and gaseous hydrogen chloride were taken from Table 5 and the CODATA Tables [39]. The calculated value is $\Delta_f H^\circ_m$(salt(cr)) = (−473 ± 8) kJ·mol^{-1}, where the expanded uncertainty (k = 2) is reported.

5. Conclusions

Condensed-phase heat capacity of crystalline rimantadine hydrochloride in a wide temperature range was measured. Decomposition of the compound was shown to be complex (at least two concurrent processes), with a simple decomposition into gaseous amine and hydrogen chloride prevailing at lower temperatures. Identification of the nature of the high-temperature decomposition requires additional study. The complexity of the decomposition did not allow determination of equilibrium partial pressures of amine and HCl, but it was possible to estimate the enthalpy of decomposition, which, together with quantum chemical calculations, gave us an estimate for the enthalpy of formation for crystalline rimantadine hydrochloride. These results are expected to be of interest for chemical engineers, either for process optimization or for development of predictive procedures for derivatives of adamantane.

Supplementary Material

Refer to Web version on PubMed Central for supplementary material.

Acknowledgement

DHZ acknowledges the financial support from DFG, grant ZA 872/3-1, 407078203. Trade names are provided only to specify procedures adequately and do not imply endorsement by the National Institute of Standards and Technology. Similar products by other manufacturers may be found to work as well or better.

References

[1]. Bagrii EI. Adamantanes: Production, properties, application; Nauka: Moscow, 1989 [in Russian]

[2]. Mansoori GA, de Araujo PLB, de Araujo ES. Diamondoid Molecules: With Applications in Biomedicine, Materials Science, Nanotechnology & Petroleum Science, 1st edition; World Scientific Publishing Co. Pte. Ltd.: New Jersey, 2012.

[3]. Wanka L, Iqbal K, Schreiner PR. The Lipophilic Bullet Hits the Targets: Medicinal Chemistry of Adamantane Derivatives. Chem Rev. 113 (2013) 3516–3604. [PubMed: 23432396]

[4]. Morozov IS, Ivanova IA, Lukicheva TA. Actoprotector and Adaptogen Properties of Adamantane Derivatives (A Review). Pharm. Chem. J 35 (2001) 235–238.

[5]. Morozov IS, Petrov VI, Sergeeva SA. Pharmacology of Adamantanes. Volgograd Medical Academy: Volgograd, 2001 [in Russian].

[6]. De Clercq E. Antiviral drugs in current clinical use. J. Clin. Virol 30 (2004) 115–133. [PubMed: 15125867]

[7]. Bazyleva A, Blokhin AV, Zaitsau DH, Kabo GJ, Paulechka E, Kazakov A, Shaw JM. Thermodynamics of the Antiviral and Antiparkinsonian Drug Amantadine Hydrochloride: Condensed State Properties and Decomposition. J. Chem. Eng. Data 62 (2017) 2666–2675.

[8]. Bazyleva AB, Blokhin AV, Kabo GJ, Charapennikau MB, Emel'yanenko VN, Verevkin SP, Diky V. Thermodynamic properties of adamantane revisited. J. Phys. Chem. B 115 (2011)10064–10072. [PubMed: 21809832]

[9]. Bazyleva AB, Blokhin AV, Kabo AG, Kabo GJ, Emel'yanenko VN, Verevkin SP. Thermodynamic properties of 1-aminoadamantane. J. Chem. Thermodyn 40 (2008) 509–522.

[10]. Karpushenkava LS, Kabo GJ, Bazyleva AB, Blokhin AV, Kabo AG, Zaitsau DH, Pimerzin AA, Sarkisova VS. Thermodynamic properties of 1,1′-biadamantane. Thermochimica Acta 459 (2007) 104–110.

[11]. Bazyleva AB, Blokhin AV, Kabo GJ, Kabo AG, Sevruk VM. Thermodynamic properties of 2-adamantanone in the condensed and ideal gaseous states. Thermochim. Acta 451 (2006) 65–72.

[12]. Bazyleva AB, Blokhin AV, Kabo GJ, Kabo AG, Paulechka YU. Thermodynamic properties of 1-bromoadamantane in the condensed state and molecular disorder in its crystals. J. Chem. Thermodyn 37 (2005) 643–657.

[13]. Charapennikau MB, Blokhin AV, Kabo AG, Kabo GJ. The heat capacities and parameters of solid phase transitions and fusion for 1- and 2-adamantanols, J. Chem. Thermodyn 35 (2003) 145–157.

[14]. Charapennikau MB, Blokhin AV, Kabo GJ, Kabo AG, Diky VV, Gusakov AG. Thermodynamic properties and the plastic crystal state of 2-methyl-2-adamantanol. Thermochim. Acta 382 (2002) 109–118.

[15]. Singer C, Papapetropoulos S, Gonzalez MA, Roberts EL, Lieberman A. Rimantadine in Parkinson's disease patients experiencing peripheral adverse effects from amantadine: Report of a case series. Mov Disord. 20 (2005) 873–877. [PubMed: 15809995]

[16]. Gerald V, Evidente H, Adler C, Caviness J, Gwinn-Hardy K. A Pilot Study on the Motor Effects of Rimantadine in Parkinson's Disease. Clin Neuropharmacol. 22 (1999) 30–32. [PubMed: 10047931]

[17]. Mishnev A, Stepanovs D. Crystal Structure Explains Crystal Habit for the Antiviral Drug Rimantadine Hydrochloride. Z. Naturforsch 69b (2014) 823–828.

[18]. Meija J, Coplen TB, Berglund M, Brand WA, De Bièvre P, Gröning M, Holden NE, Irrgeher J, Loss RD, Walczyk T, Prohaska T, Atomic weights of the elements 2013. IUPAC Technical Report. Pure Appl. Chem 88 (2016) 265–291.

[19]. Blokhin AV, Paulechka YU, Kabo GJ. Thermodynamic Properties of $[C_6mim][NTf_2]$ in the Condensed State. J. Chem. Eng. Data 51 (2006) 1377–1388.

[20]. Ginnings DC, Furukawa GT. Heat Capacity Standards for the Range 14 to 1200 K. J. Am. Chem. Soc 75 (1953) 522–527.

[21]. Zaitsau DH, Kabo GJ, Strechan AA, Paulechka YU, Tschersich A, Verevkin SP, Heintz A. Experimental Vapor Pressures of 1-Alkyl-3-methylimidazolium Bis(trifluoromethylsulfonyl)imides and a Correlation Scheme for Estimation of Vaporization Enthalpies of Ionic Liquids. J. Phys. Chem. A 110 (2006) 7303–7306. [PubMed: 16737284]

[22]. Becke AD, Density-Functional Thermochemistry. III. The Role of Exact Exchange. J. Chem. Phys 98 (1993) 5648–5652.

[23]. Stephens PJ, Devlin FJ, Chabalowski CF, Frisch MJ. Ab Initio Calculation of Vibrational Absorption and Circular Dichroism Spectra Using Density Functional Force Fields. J. Phys. Chem 98 (1994) 11623–11627.

[24]. Weigend F, Ahlrichs R. Balanced basis sets of split valence, triple zeta valence and quadruple zeta valence quality for H to Rn: Design and assessment of accuracy. Phys. Chem. Chem. Phys 7 (2005) 3297–3305. [PubMed: 16240044]

[25]. Grimme S, Ehrlich S, Goerigk L. Effect of the damping function in dispersion corrected density functional theory. J. Comput. Chem 32 (2011) 1456–1465. [PubMed: 21370243]

[26]. Nagy PR, Kállay M. Optimization of the linear-scaling local natural orbital CCSD(T) method: Redundancy-free triples correction using Laplace transform. J. Chem. Phys 146 (2017)214106 [PubMed: 28576082]

[27]. Nagy PR, Samu G, Kállay M. An Integral-Direct Linear-Scaling Second-Order Møller-Plesset Approach. J. Chem. Theory Comput 12 (2016) 4897–4914. [PubMed: 27618512]

[28]. Kállay M, Nagy PR, Rolik Z, Mester D, Samu G, Csontos J, Csóka J, Szabó BP, Gyevi-Nagy L, Ladjánszki I, Szegedy L, Ladóczki B, Petrov K, Farkas M, Mezei PD, and Hégely B. MRCC, a Quantum Chemical Program Suite, 2018. https://www.mrcc.hu, accessed October 21, 2019.

[29]. Dunning TH. Gaussian basis sets for use in correlated molecular calculations. I. The atoms boron through neon and hydrogen. J. Chem. Phys 90 (1989) 1007–1023.

[30]. Kendall RA, Dunning TH, Harrison RJ. Electron affinities of the first-row atoms revisited. Systematic basis sets and wave functions. J. Chem. Phys 96 (1992) 6796–6806.

[31]. Dunning TH, Peterson KA, Wilson AK. Gaussian basis sets for use in correlated molecular calculations. X. The atoms aluminum through argon revisited. J. Chem. Phys 114 (2001)9244–9253.

[32]. Woon DE, Dunning TH. Gaussian basis sets for use in correlated molecular calculations. III. The atoms aluminum through argon. J. Chem. Phys 98 (1993) 1358–1371.

[33]. Frisch MJ, Trucks GW, Schlegel HB, Scuseria GE, Robb MA, Cheeseman JR, Scalmani G, Barone V, Petersson GA, Nakatsuji H, Li X, Caricato M, Marenich AV, Bloino J, Janesko BG, Gomperts R, Mennucci B, Hratchian HP, Ortiz JV, Izmaylov AF, Sonnenberg JL, Williams-Young D, Ding F, Lipparini F, Egidi F, Goings J, Peng B, Petrone A, Henderson T, Ranasinghe D, Zakrzewski VG, Gao J, Rega N, Zheng G, Liang W, Hada M, Ehara M, Toyota K, Fukuda R, Hasegawa J, Ishida M, Nakajima T, Honda Y, Kitao O, Nakai H, Vreven T, Throssell K, Montgomery JA Jr., Peralta JE, Ogliaro F, Bearpark MJ, Heyd JJ, Brothers EN, Kudin KN, Staroverov VN, Keith TA, Kobayashi R, Normand J, Raghavachari K, Rendell AP, Burant JC, Iyengar SS, Tomasi J, Cossi M, Millam JM, Klene M, Adamo C, Cammi R, Ochterski JW, Martin RL, Morokuma K, Farkas O, Foresman JB, Fox DJ. Gaussian 16, Revision B.01, Gaussian, Inc., Wallingford CT, 2016.

[34]. McQuarrie DA. Statistical Mechanics. University Science Books: Sausalito, CA, 2000.

[35]. Pitzer KS. Energy Levels and Thermodynamic Functions for Molecules with Internal Rotation: II. Unsymmetrical Tops Attached to a Rigid Frame. J. Chem. Phys 14 (1946) 239–243.

[36]. Paulechka E, Kazakov A. Efficient Estimation of Formation Enthalpies for Closed-Shell Organic Compounds with Local Coupled-Cluster Methods. J. Chem. Theory Comput 14 (2018) 5920–5932. [PubMed: 30234978]

[37]. Paulechka E, Kazakov A. Efficient DLPNO–CCSD(T)-Based Estimation of Formation Enthalpies for C-, H-, O-, and N-Containing Closed-Shell Compounds Validated Against Critically Evaluated Experimental Data. J. Phys. Chem. A 122 (2017) 4379–4387.

[38]. Bélanger-Gariépy F, Brisse F, Harvey PD, Butler IS, Gilson DFR. Structure of adamantanamine hydrochloride at 143 K. Acta Cryst. C43 (1987) 756–759.

[39]. Cox JD, Wagman DD, Medvedev VA. CODATA Key Values for Thermodynamics; Hemisphere Publishing Corp.: New York, 1989.

[40]. Li J, Kazakov A, Dryer FL. Experimental and Numerical Studies of Ethanol Decomposition Reactions. J. Phys. Chem. A 108 (2004) 7671–7680.

[41]. van Duijneveldt FB, van JGCM de Rijdt Duijneveldt-van, van Lenthe JH. State of the Art in Counterpoise Theory. Chem. Rev 94 (1994) 1873–1885.

Highlights

- Heat capacity of crystalline rimantadine hydrochloride was measured from (7 to 453) K.
- Thermodynamic functions for rimantadine hydrochloride were derived.
- Decomposition of rimantadine hydrochloride into amine and HCl was probed.
- Ideal-gas properties of the amine were calculated.
- Enthalpy of formation of the salt was estimated.

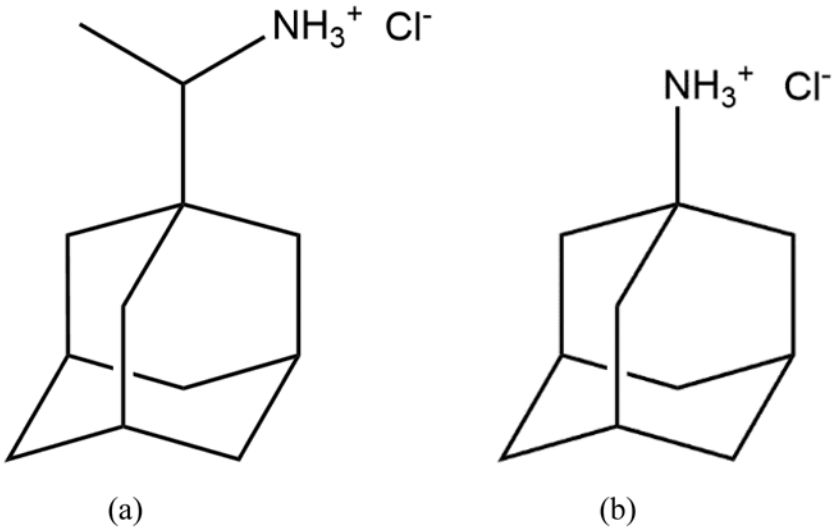

FIGURE 1.
Structures of rimantadine hydrochloride (a) and amantadine hydrochloride (b)

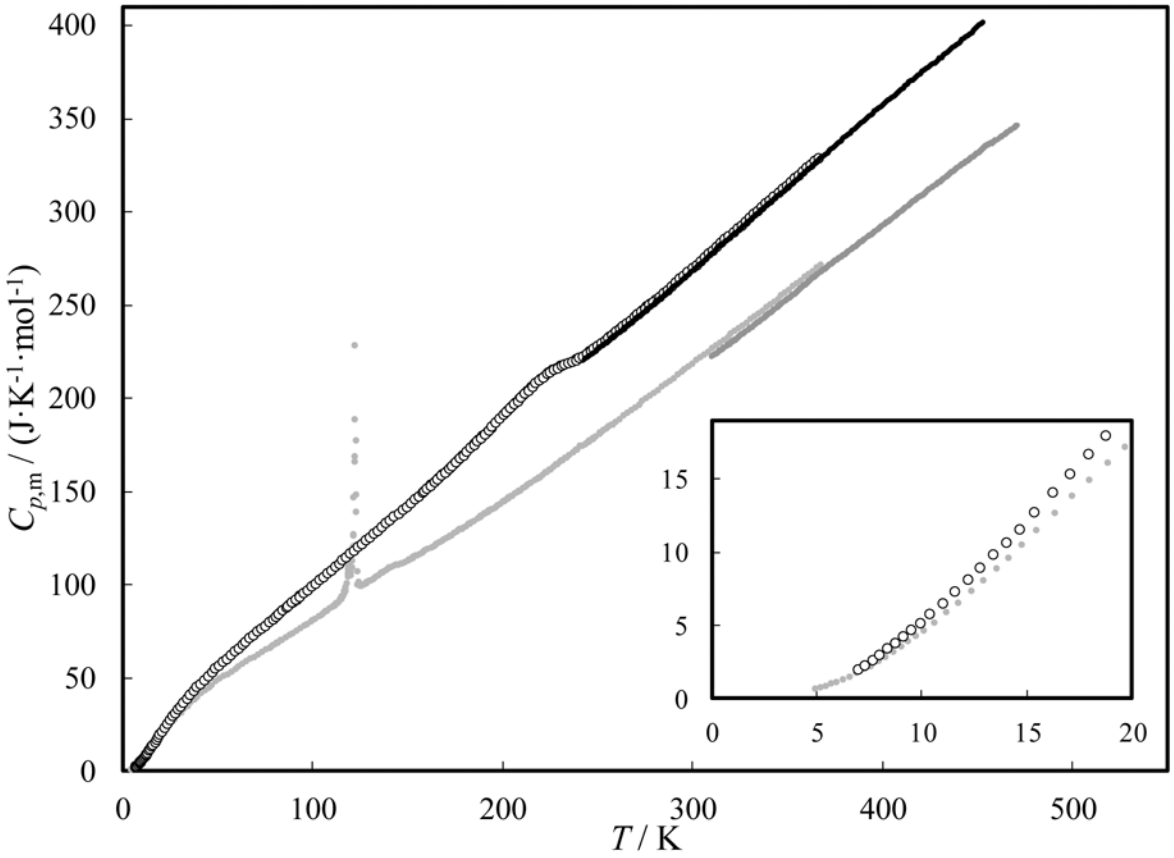

FIGURE 2.

Temperature dependence of isobaric heat capacities of crystalline rimantadine hydrochloride from this work (black empty circles, adiabatic calorimetry; solid black line, DSC) and amantadine hydrochloride from previous work [7] (grey filled circles, adiabatic calorimetry; solid grey line, DSC). Inset: enlarged low-temperature region.

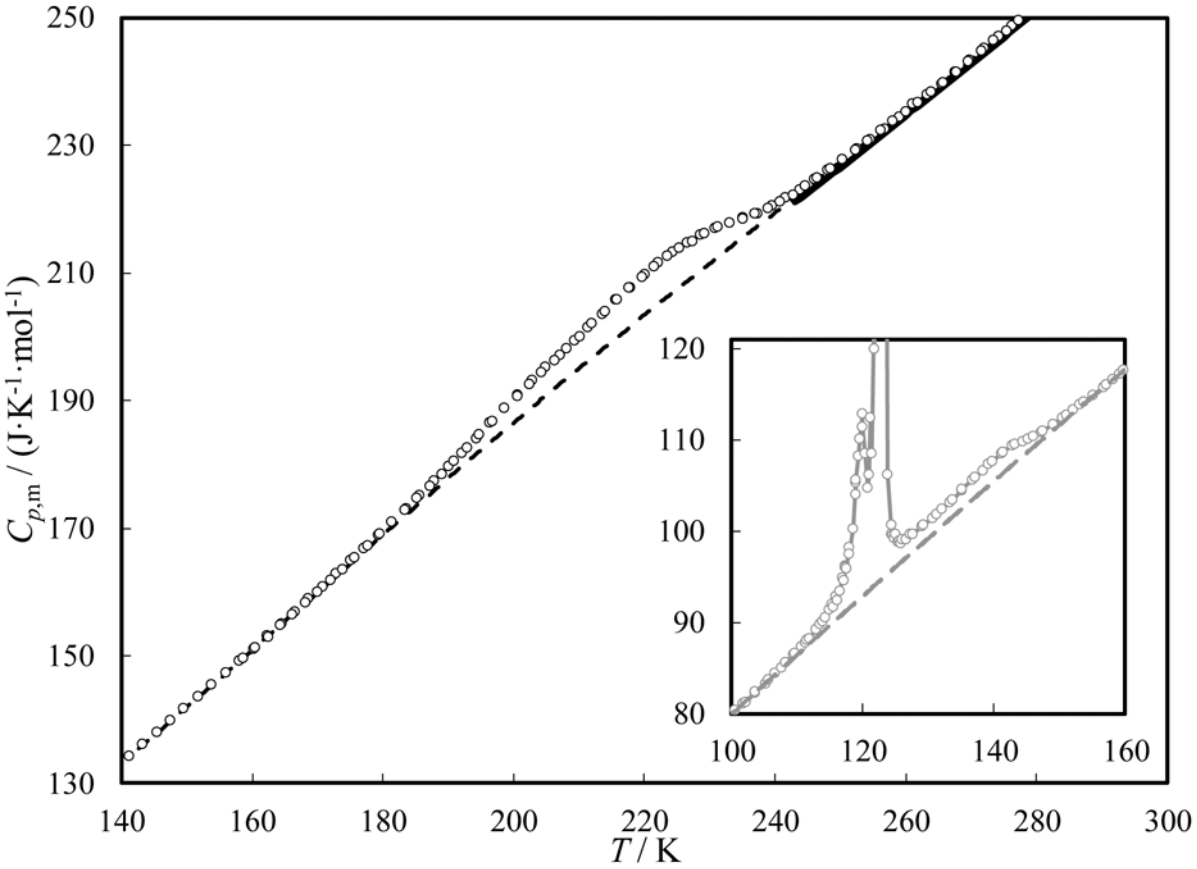

FIGURE 3.

Heat-capacity baseline selected for calculation of excess enthalpy and excess entropy of the hump-like phase anomaly. Main graph: rimantadine hydrochloride (empty circles, adiabatic calorimetry; solid line, DSC; dashed line, C_p baseline). Inset: amantadine hydrochloride [7] (empty circles, adiabatic calorimetry; dashed line, C_p baseline)

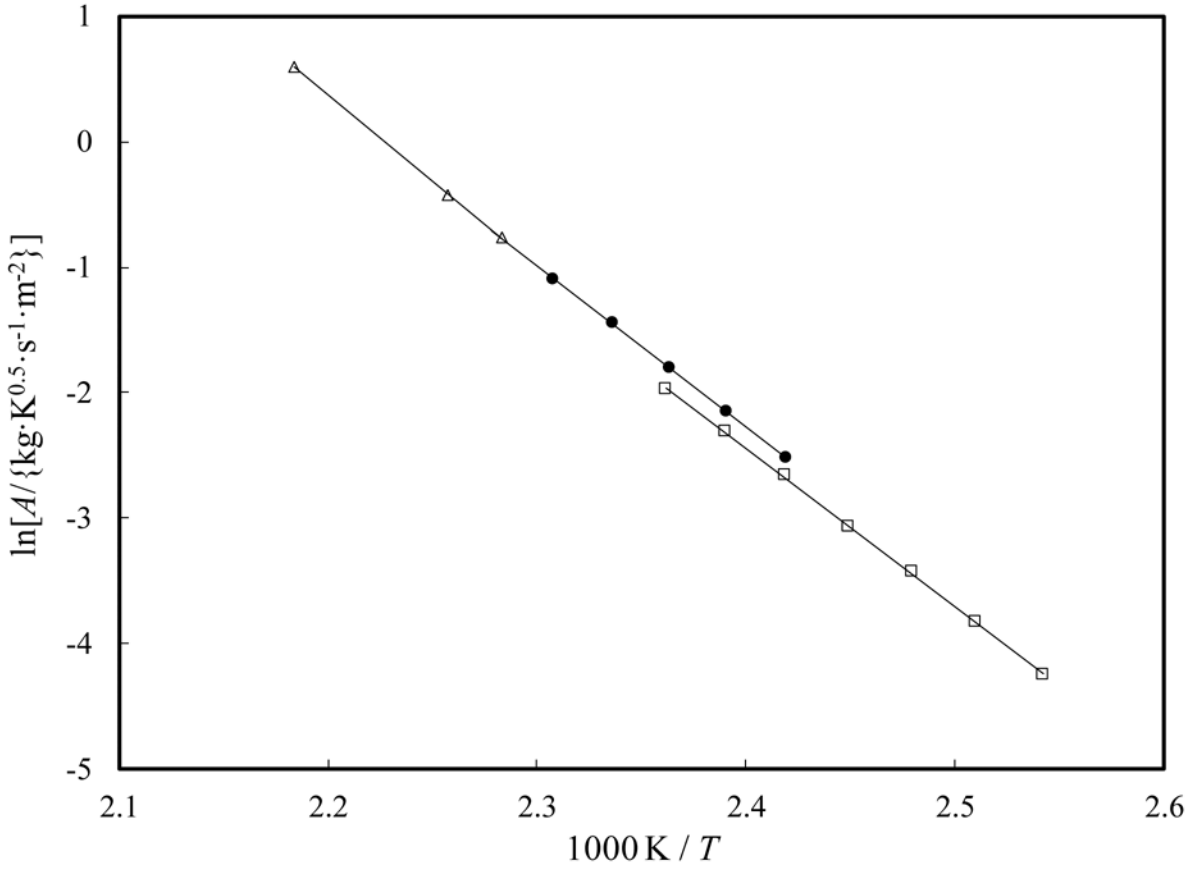

FIGURE 4.

Temperature dependence of $A = \sqrt{T}\,(\Delta m / \tau)\, S_{or}^{-1}$ obtained with the use of membranes with different orifice diameters: Δ, d_{or} = 0.183 mm; ●, d_{or} = 0.447 mm; □, d_{or} = 0.837 mm.

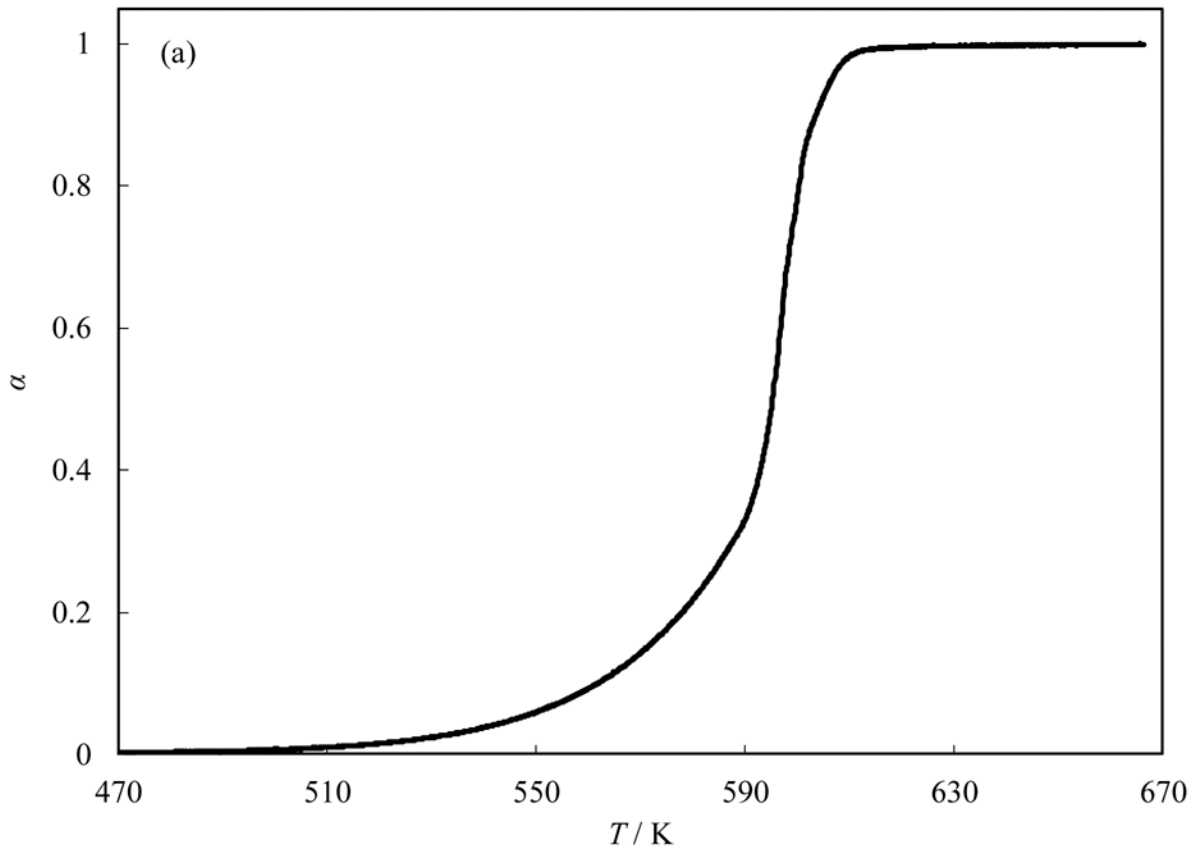

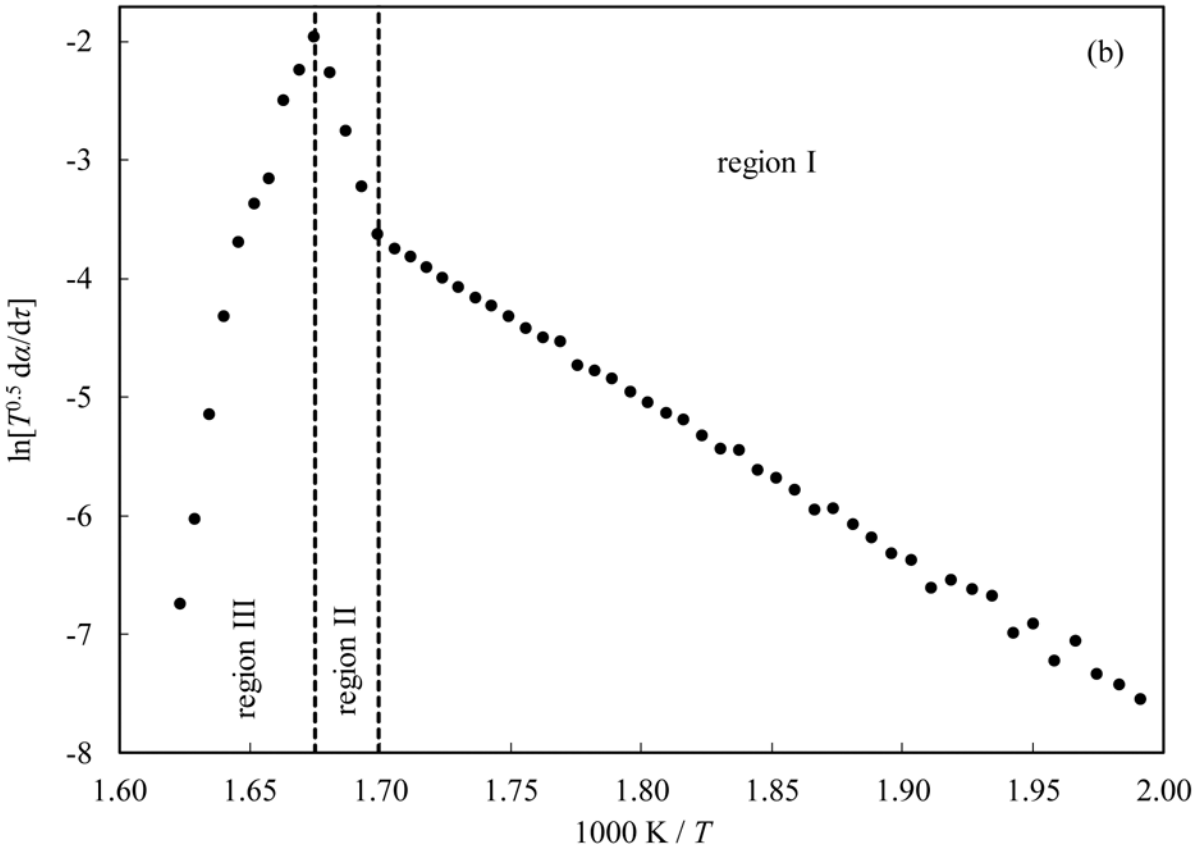

FIGURE 5.

Typical TGA curve for rimantadine hydrochloride (5 K·min^{-1}): (a) degree of decomposition α as a function of temperature; (b) scaled reaction rate in the Arrhenius coordinates. Region I corresponds to the supposed low-temperature equilibrium between crystal and gas phases. The high-temperature decomposition is a major process in region II. The decreased reaction rate in region III is due to the sample depletion.

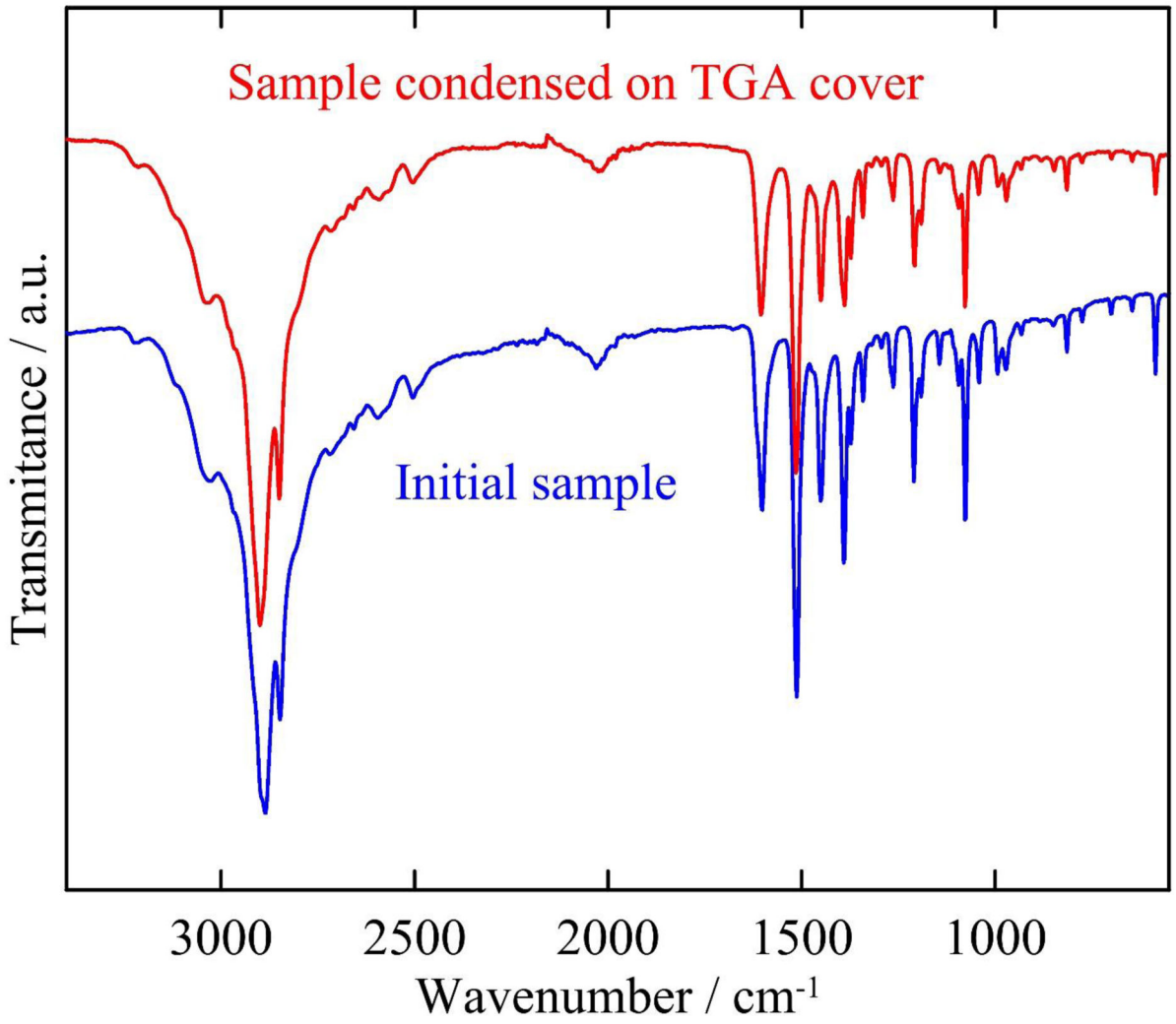

FIGURE 6.

The results of FTIR-ATR analysis of the rimantadine hydrochloride used in the TGA study (5 K·min^{-1}) in Figure 5.

TABLE 1.

Sample description table

Chemical Name (CAS registry number)	Source	Initial Mass-Fraction Purity	Purification
Rimantadine hydrochloride (1501-84-4)	RUE “Belmedpreparaty” (Minsk, Belarus)	0.99 [a]	Vacuum treatment
Rimantadine hydrochloride (1501-84-4)	Acros Organics (ThermoFisher Scientific, Lot 75749)	0.95 [a]	Vacuum treatment
Benzoic acid (65-85-0)	Parr Instrument Company	0.9999 [a]	No additional treatment

[a]Stated by the supplier. No additional purity analysis was performed.

TABLE 2.

Smoothed standard molar thermodynamic functions of rimantadine hydrochloride (M = 215.765 g·mol^{-1}) in the crystalline state at standard pressure of 10^5 Pa [a,b]

T /K	$C^{o}_{p,m}$	$\Delta_0^T H^{o}_m / T$	$\Delta_0^T S^{o}_m$	Φ^{o}_m
	J·K^{-1}·mol^{-1}			
5	0.729 ± 0.015	0.1822 ± 0.0036	0.2429 ± 0.0049	0.0607 ± 0.0012
10	5.142 ± 0.075	1.386 ± 0.024	1.865 ± 0.033	0.4785 ± 0.0083
15	12.05 ± 0.11	3.750 ± 0.049	5.208 ± 0.072	1.458 ± 0.020
20	19.68 ± 0.08	6.787 ± 0.062	9.729 ± 0.102	2.942 ± 0.029
25	27.05 ± 0.11	10.11 ± 0.07	14.92 ± 0.12	4.810 ± 0.036
30	33.76 ± 0.14	13.50 ± 0.08	20.46 ± 0.14	6.954 ± 0.044
35	39.80 ± 0.16	16.83 ± 0.09	26.12 ± 0.17	9.287 ± 0.054
40	45.31 ± 0.18	20.05 ± 0.10	31.80 ± 0.19	11.75 ± 0.06
45	50.47 ± 0.20	23.15 ± 0.11	37.44 ± 0.21	14.29 ± 0.07
50	55.36 ± 0.22	26.13 ± 0.12	43.01 ± 0.23	16.88 ± 0.08
60	64.58 ± 0.26	31.78 ± 0.14	53.93 ± 0.28	22.15 ± 0.11
70	73.33 ± 0.29	37.09 ± 0.16	64.55 ± 0.32	27.45 ± 0.13
80	81.90 ± 0.33	42.16 ± 0.18	74.90 ± 0.36	32.74 ± 0.15
90	90.44 ± 0.36	47.05 ± 0.20	85.04 ± 0.40	37.99 ± 0.17
100	99.01 ± 0.40	51.82 ± 0.21	95.01 ± 0.44	43.19 ± 0.19
110	107.6 ± 0.4	56.50 ± 0.23	104.8 ± 0.5	48.35 ± 0.21
120	116.1 ± 0.5	61.11 ± 0.25	114.6 ± 0.5	53.47 ± 0.23
130	124.6 ± 0.5	65.66 ± 0.27	124.2 ± 0.6	58.54 ± 0.25
140	133.2 ± 0.5	70.18 ± 0.29	133.8 ± 0.6	63.57 ± 0.27
150	142.0 ± 0.6	74.68 ± 0.30	143.2 ± 0.6	68.56 ± 0.29
160	150.9 ± 0.6	79.16 ± 0.32	152.7 ± 0.7	73.53 ± 0.31
170	160.0 ± 0.6	83.64 ± 0.34	162.1 ± 0.7	78.46 ± 0.33
180	169.5 ± 0.7	88.15 ± 0.36	171.5 ± 0.7	83.37 ± 0.35
190	179.5 ± 0.7	92.69 ± 0.37	180.9 ± 0.8	88.26 ± 0.37
200	190.1 ± 0.8	97.30 ± 0.39	190.4 ± 0.8	93.13 ± 0.39
210	200.0 ± 0.8	102.0 ± 0.4	199.9 ± 0.9	97.99 ± 0.41
220	209.6 ± 0.8	106.6 ± 0.4	209.5 ± 0.9	102.8 ± 0.4
230	216.5 ± 0.9	111.3 ± 0.4	219.0 ± 0.9	107.7 ± 0.4
240	220.7 ± 0.9	115.7 ± 0.5	228.3 ± 1.0	112.5 ± 0.5
250	227.4 ± 0.9	120.1 ± 0.5	237.4 ± 1.0	117.3 ± 0.5
260	235.2 ± 0.9	124.4 ± 0.5	246.5 ± 1.0	122.1 ± 0.5
270	243.4 ± 1.0	128.6 ± 0.5	255.5 ± 1.1	126.9 ± 0.5
280	251.8 ± 1.0	132.9 ± 0.5	264.5 ± 1.1	131.6 ± 0.5
290	260.3 ± 1.0	137.1 ± 0.6	273.5 ± 1.2	136.4 ± 0.6
298.15	267.5 ± 1.1	140.6 ± 0.6	280.8 ± 1.2	140.2 ± 0.6
300	269.2 ± 1.1	141.4 ± 0.6	282.5 ± 1.2	141.1 ± 0.6

T /K	$C^{o}_{p,m}$	$\Delta^{T}_{0}H^{o}_{m}/T$	$\Delta^{T}_{0}S^{o}_{m}$	Φ^{o}_{m}
	J·K^{-1}·mol^{-1}			
310	278.1 ± 1.1	145.6 ± 0.6	291.4 ± 1.2	145.8 ± 0.6
320	287.1 ± 1.1	149.9 ± 0.6	300.4 ± 1.3	150.5 ± 0.6
330	296.1 ± 1.2	154.2 ± 0.6	309.4 ± 1.3	155.2 ± 0.6
340	305.0 ± 1.2	158.5 ± 0.6	318.3 ± 1.3	159.8 ± 0.7
350	313.9 ± 1.3	162.8 ± 0.7	327.3 ± 1.4	164.5 ± 0.7
360	322.6 ± 1.3	167.1 ± 0.7	336.3 ± 1.4	169.1 ± 0.7
370	331.3 ± 1.3	171.5 ± 0.7	345.2 ± 1.4	173.8 ± 0.7
380	340 ± 7	175.8 ± 0.8	354.2 ± 1.6	178.4 ± 0.8
390	349 ± 7	180.1 ± 1.0	363.1 ± 1.8	183.0 ± 1.0
400	357 ± 7	184.4 ± 1.2	372.1 ± 2.0	187.6 ± 1.1
410	366 ± 7	188.7 ± 1.3	381.0 ± 2.2	192.3 ± 1.2
420	374 ± 7	193.1 ± 1.4	389.9 ± 2.3	196.9 ± 1.3
430	382 ± 8	197.4 ± 1.6	398.8 ± 2.5	201.4 ± 1.4
440	391 ± 8	201.7 ± 1.7	407.7 ± 2.7	206.0 ± 1.6
450	399 ± 8	206.0 ± 1.9	416.6 ± 2.9	210.6 ± 1.7
453	402 ± 8	207.2 ± 1.9	419.2 ± 2.9	212.0 ± 1.7

[a] Expanded uncertainties with 0.95 confidence level are reported inside the table.

[b] $C^{o}_{p,m}$ is the molar isobaric heat capacity, $\Delta^{T}_{0}H^{o}_{m}/T$ is the reduced enthalpy relative to 0 K, $\Delta^{T}_{0}S^{o}_{m}$ is the entropy relative to 0 K, $\Phi^{o}_{m} = \Delta^{T}_{0}S^{o}_{m} - \Delta^{T}_{0}H^{o}_{m}/T$.

TABLE 3.

Mass-loss data in effusion experiments with crystalline rimantadine hydrochloride [a,b]

Point #	d_{or} / mm	l / μm	T / K	τ / s	Δm / mg
1	0.8370	50	408.27	16200	20.39
2	0.8370	50	403.27	10800	9.55
3	0.8370	50	398.39	16200	9.73
4	0.8370	50	393.36	21600	8.57
5	0.8370	50	413.38	5400	10.20
6	0.8370	50	418.36	4200	11.15
7	0.8370	50	423.36	3600	13.42
8	0.4467	72	433.26	5400	13.56
9	0.4467	72	413.30	16200	10.00
10	0.4467	72	418.28	12000	10.68
11	0.4467	72	423.09	8100	10.14
12	0.4467	72	428.00	5400	9.58
13	0.1833	50	457.94	5400	12.14
14	0.1833	50	438.03	18000	10.62
15	0.1833	50	438.03	12600	10.34

[a] Δm is the experimental sample mass loss from effusion cell into the vacuum during time τ at temperature T; l is the membrane thickness, and d_{or} is the effusion orifice diameter.

[b] Standard uncertainties u are u(T) = 0.05 K, $u(d_{or})$ = 0.0005 mm, $u(l)$ = 1 μm, u(Δm) = 0.02 mg, u(τ) = 5 s.

TABLE 4.

Characteristics of conformers for rimantadine and rimantadine hydrochloride [a]

Conformer	Structure	$10^{135} I_A I_B I_C$ / kg^3·m^6	ΔE(0 K) / kJ·mol^{-1}	ZPVE / kJ·mol^{-1}	ΔH(298 K) / kJ·mol^{-1}
Rimantadine					
1	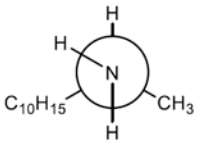	956.5	1.87	822.83	1.83
2	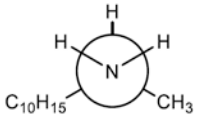	943.7	0.00	823.99	0.00
3	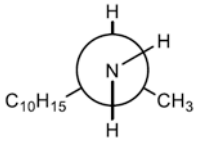	945.7	1.98	822.67	1.74
Rimantadine hydrochloride					
1	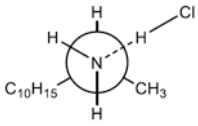	5189	0.00	847.53	0.00
2	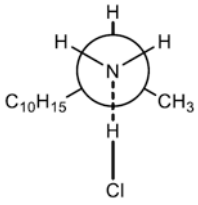	3802	−0.07	851.29	2.85
3	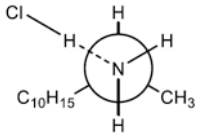	3899	4.61	850.82	7.22

[a] ΔE(0 K) is the total energy of a conformer relative to the most stable one at 0 K; $I_A I_B I_C$ is the product of moments of inertia; ZPVE is the zero-point vibrational energy; ΔH(298 K) is the relative enthalpy of a conformer at 298.15 K.

TABLE 5.

Thermodynamic properties of rimantadine (for a single enantiomer) in the ideal-gas state ($p° = 10^5$ Pa)

T / K	$C^{o}_{p,m}$	$\Delta_0^T H^{o}_m / T$	$\Delta_0^T S^{o}_m$	$\Delta_f H°_m$	$\Delta_f G°_m$
	J·K^{-1}·mol^{-1}			kJ mol^{-1}	
0	0.0	0.0	0.0	−96.3	−96.3
50	46.5	36.9	247.1	−109.6	−77.6
100	77.7	49.5	288.9	−125.0	−39.0
150	109.1	64.1	326.3	−136.7	6.6
200	142.7	79.5	362.2	−147.8	56.0
273.15	199.0	103.8	414.8	−163.5	133.1
298.15	219.7	112.6	433.1	−168.6	160.5
300	221.2	113.3	434.5	−169.0	162.5
400	303.5	150.7	509.5	−186.9	275.8
500	376.5	188.7	585.3	−200.9	393.2
600	437.4	225.3	659.5	−211.3	513.1
700	487.9	259.3	730.8	−218.6	634.5
800	530.0	290.6	798.8	−223.3	757.3
900	565.5	319.2	863.3	−225.7	879.3
1000	595.6	345.4	924.5	−226.2	1002.2